ACS Photonics

Article

pubs.acs.org/journal/apchd5

Light-Triggered Control of Plasmonic Refraction and Group Delay by Photochromic Molecular Switches

Malte Großmann,[*,†] Alwin Klick,[†] Christoph Lemke,[†] Julian Falke,[†] Maximilian Black,[†] Jacek Fiutowski,[‡] Arkadiusz Jaroslaw Goszczak,[‡] Elzbieta Sobolewska,[‡] Ahnaf Usman Zillohu,[§] Mehdi Keshavarz Hedayati,[∥] Horst-Guenter Rubahn,[‡] Franz Faupel,[⊥] Mady Elbahri,[§,∥,¶] and Michael Bauer[†]

[†]Institute of Experimental and Applied Physics, University of Kiel, Leibnizstraße 19, D-24118 Kiel, Germany

[‡]Mads Clausen Institute, NanoSYD, University of Southern Denmark, Alsion 2, DK-6400 Sønderborg, Denmark

[§]Nanochemistry and Nanoengineering, Institute of Polymer Research, Helmholtz Zentrum Geesthacht, Max Planck Straße 1, D-21502 Geesthacht, Germany

[∥]Nanochemistry and Nanoengineering and [⊥]Multicomponent Materials, Institute for Materials Science, Faculty of Engineering, University of Kiel, Kaiserstrasse 2, D-24143 Kiel, Germany

[¶]Nanochemistry and Nanoengineering, School of Chemical Technology, Aalto University, Helsinki, Kemistintie 1, 02150 Espoo, Finland

ABSTRACT: An interface supporting plasmonic switching is prepared from a gold substrate coated with a polymer film doped with photochromic molecular switches. A reversible light-induced change in the surface plasmon polariton dispersion curve of the interface is experimentally demonstrated, evidencing reversible switching of the surface plasmon polariton group and phase velocity. The switching capabilities of the interface are furthermore successfully applied to achieve focus control of a plasmonic lens. The results imply the realization of nonvolatile and reversible plasmonic switching units providing complex functionalities based on surface plasmon refraction and group delay.

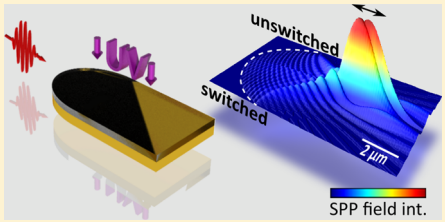

KEYWORDS: *active plasmonics, plasmonic devices, photochromic molecular switches*

Plasmonic devices employing localized surface plasmons (LSPs) and surface plasmon polaritons (SPPs) are a focus of recent research because of their prospect for combining the speed of photonics with the capabilities of miniaturization of electronics.[1−3] As a vision for potential applications, plasmon-based devices could be utilized for instance in future-generation on-chip communication and signal processing.[4−6] Due to these prospects plasmonic excitations and their interaction with nanoscale systems have attracted considerable interest, and a multitude of related phenomena have been studied in the recent past including coherence and nonlinearities in localized plasmonic excitations,[7−9] control of plasmonic near fields by means of pulse-shaping techniques,[10] plasmon wave packet propagation along metal−dielectric interfaces,[11−14] and plasmonic coupling to quantum emitters.[15,16]

Signal switching, modulation, and amplification during operation of plasmonic devices rely on the development of schemes by which the plasmonic response can be controlled actively and in a reversible manner. Promising routes toward the realization of such schemes involve the use of appropriate material functionalities. In the past active plasmonic circuits have successfully been realized using phase-change materials,[17] thermal changes in plasmonic waveguide media,[18,19] interactions mediated by quantum dots,[20] nonlinear interactions between a propagating SPP and light,[4] stimulated emission of copropagating SPPs,[21] and electro-optical field effects.[22]

Photochromic molecular switches undergo reversible and stable changes in their optical properties when irradiated by light of a specific wavelength.[23−25] Both LSPs and SPPs react very sensitively to changes in the permittivity of the dielectric environment, so that one can expect this type of functionality to be useful for the fabrication of active plasmonic circuits that are controlled by an external optical stimulus. In contrast to many other schemes, this approach shows the advantage of a nonvolatile behavior; that is, there is no need of a continuous supply power to maintain a "nonequilibrium" switching state. On the basis of this concept, Pala et al. realized a plasmonic switch that exploits the sensitivity of the SPP propagation length (i.e., the imaginary part k''_{SPP} of the SPP wave vector) to changes in the imaginary part k of the refractive index of a poly(methyl methacrylate) (PMMA) film, doped with photochromic spiropyran molecules.[26] Notably, in a recent work very similar results were reported for a plasmonic waveguide using the switching capabilities of a phase change material.[27] Changes in the permittivity of the dielectric environment affect also the real part k'_{SPP} of the SPP wave vector, i.e., SPP phase velocity v_p and the SPP group velocity v_g, providing a means of controlling SPP refraction and SPP group delay. This property permits new types of active plasmonic units built from photochromic

Received: June 5, 2015
Published: August 18, 2015

DOI: 10.1021/acsphotonics.5b00315
ACS Photonics 2015, 2, 1327−1332

dielectrics, such as light-triggered plasmonic delay lines and adaptive plasmonic lenses.

In this work, we provide experimental proof for the light-induced and reversible control of k'_{SPP} at the interface of a gold film and a dielectric made from a polymeric matrix doped with photochromic molecular switches. Using two-photon photoemission electron microscopy (2P-PEEM) in a spectroscopic operation mode,[28] changes in k'_{SPP} of up to 0.2 μm^{-1} are observed over a wide range of the SPP dispersion relation $k'_{SPP}(\omega)$, with ω being the plasmon frequency. A quantitative comparison of these results with values based on ellipsometry data confirms that the changes in the plasmonic response result from the light-induced changes in the permittivity of the dielectric film, i.e., from the switching of the photochromic molecules. On the basis of this concept we realize a switchable plasmonic lens as a first demonstrator for potential applications. Reversible focus control is experimentally demonstrated, yielding changes of about 5% of the total focal length.

EXPERIMENTAL SECTION

The experiments on SPP switching were conducted using a photoemission electron microscope (IS PEEM, Focus GmbH)[29] mounted in an ultra-high-vacuum (UHV) μ-metal chamber and providing a lateral resolution of better than 40 nm. The samples were excited under a fixed angle of incidence (65°) toward the surface normal by transform-limited laser pulses (~100 fs pulse width) from a Ti:sapphire oscillator operated at a repetition rate of 80 MHz (Tsunami, Spectra Physics). The central wavelength of the laser is continuously tunable between 710 and 890 nm, and it was measured using a calibrated fiber-optic spectrometer (USB400, Ocean Optics) in front of the UHV chamber entrance window. Prior to the photoemission measurements, the samples were covered with a small amount of cesium (coverage $\ll$1) in the UHV chamber using a well-degassed SAES getter source. This treatment is required to lower the work function in order to facilitate a two-photon photoemission process with near-infrared light pulses. SPP propagation (real and imaginary part of the SPP wave vector) is not affected in the applied coverage regime within the resolution of our experiment.[28] Optical microscopy (Leica DM 2500) and conventional threshold PEEM ($h\nu$ = 4.9 eV) were used for characterization of the sample topography. To avoid unintended degradation of the samples upon illumination with UV light, conventional threshold PEEM images were taken only after the switching experiments were completed. For switching and back-switching of the photochromic molecules we use 365 nm light from a light-emitting diode (LEDMO-D365.140.OEM by Omicron Laserage) and 532 nm light from a continuous-wave laser (MGL-III-532 by CNI), respectively. Ellipsometry data were taken with a J.A. Woollam Co., Inc. M2000 UI (spectroscopic ellipsometer) with a dual-lamp system with deuterium and quartz tungsten halogen (QTH) lamps as the light sources.

The software used to control the CCD camera of the PEEM is μManager.[30] Analysis of the PEEM images was carried out using the program Fiji.[31]

The photoswitchable dielectric used in the present study was fabricated by dispersing spirophenanthrooxazine (1,3-dihydro-1,3,3-trimethylspiro[2*H*-indole-2,3′-[3*H*]phenanthr[9,10-*b*]-(1,4)oxazine]) (SPO) molecules in a polystyrene (PS) matrix. SPO is a photochromic molecular switch, which undergoes a ring-opening reaction at illumination with ultraviolet (UV) light, as illustrated schematically in Figure 1a.[24] The back-reaction can be induced either with light in the visible spectral regime or by thermal activation. The striking switching capabilities of the PS/SPO composite were proven in recent works on the demonstration of a photoswitchable transparent conductor[32] and on the construction of novel dynamic metamaterials.[33] The changes in the optical properties of PS/SPO in response to a UV light stimulus were determined from ellipsometry data from a 40 nm thick PS/SPO film (filling factor of 50 wt % SPO) on a glass substrate. Values for the real part n and the imaginary part k of the refractive index of the PS/SPO film in the two switching states based on the ellipsometry measurement are shown in Figure 1c. The experiments on SPP switching, which are discussed below, were performed at a laser excitation wavelength λ between 710 and 890 nm. Notably, in this wavelength regime (see highlighted red area in Figure 1c), significant changes are observed for n.

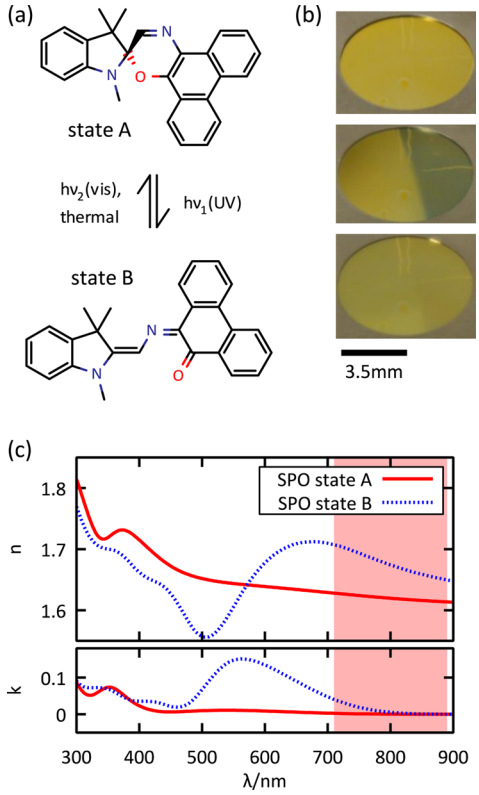

Figure 1. (a) Illustration of the SPO molecule in its ring-closed (state A) and ring-opened (state B) forms;[24] illumination of the molecule in state A with UV light ($h\nu_1$) causes cleavage of the C_{sp^3}–oxygen bond as well as flattening and isomerization of the molecule into state B. State B can relax back into state A by absorbing light in the visible spectral regime ($h\nu_2$) or by thermal activation. (b) Optical response of a PS/SPO film deposited onto a prestructured gold/silicon substrate in the two SPO switching states (the sample is already mounted in a PEEM sample holder); top image: before switching; center image: after illumination of the right-hand side of the sample with 365 nm light; bottom image: after thermal treatment of the entire sample; (c) real and imaginary part of the refractive index, n and k, as determined for a 40 nm thick PS/SPO film (filling factor of 50 wt % SPO) deposited onto a glass substrate from ellipsometry data for the two SPO switching states; the solid lines show the refractive index before switching by illumination with UV light; the dashed lines, after switching by illumination with UV light. The highlighted red area indicates the wavelength regime available in the present study for SPP excitation.

DOI: 10.1021/acsphotonics.5b00315
ACS Photonics 2015, 2, 1327–1332

SPP-supporting samples were made from silicon substrates covered with 100 nm thick gold films. In order to achieve efficient SPP excitation by light, quadratic platforms of silicon ($100 \times 100\ \mu m^2$, 100 nm height) were first fabricated by UV photolithography and reactive-ion etching. The polycrystalline gold film with a titanium adhesion layer was evaporated on top of the prestructured silicon substrate. On illumination with light the defined edges of the platforms act as a momentum source to overcome the wave vector mismatch between light and the SPP. PS/SPO films (filling factor of 40 wt % SPO) were deposited on top of the gold films by spin coating. Surface profilometry measurements yielded a PS/SPO film thickness of 60 ± 10 nm. The switching capabilities of the PS/SPO films after deposition were double-checked by directly viewing the optical response of the sample at illumination with UV light and after thermal treatment (see Figure 1b). A schematic overview of sample geometry and experimental configuration is shown in Figure 2.

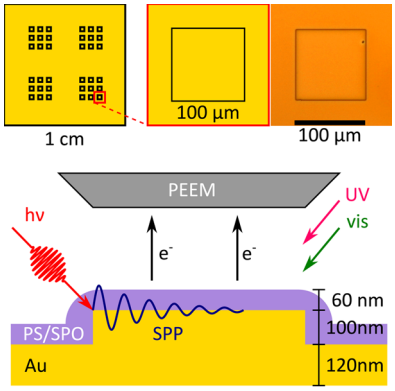

Figure 2. Top: Schematic view of sample geometry: overview of the entire sample carrying a total of 36 coupling platforms (left), zoom-in on a single gold platform (middle), and optical microscopy image of a single platform (right). Bottom: Schematic view of experimental configuration; "$h\nu$" marks the incident laser pulse used for SPP excitation. Photoemitted electrons (e^-) are collected by the PEEM entrance lense. "UV" and "vis" mark the pathways of the light used for switching and back-switching; thicknesses of the gold film, gold platform, and the PS/SPO overlayer are given on the bottom right.

RESULTS AND DISCUSSION

Figure 3a shows an image of part of an SPP coupling platform recorded in a conventional threshold PEEM on illumination with UV light (λ = 253 nm). At this frequency the gold-PS/SPO interface does not support SPP modes, so that SPP excitation is not possible. The observed contrast reflects the pure platform geometry. The identical sample area, now monitored in the 2P-PEEM mode, is shown in Figure 3b. For excitation, the sample is illuminated with laser light (λ = 730 nm) incident from the left. The image contrast has completely changed and is now dominated by an evanescent periodic photoemission intensity pattern emerging from the left edge of the SPP coupling platform, marked by the dashed line. The pattern is due to the emission of SPPs that are excited by coupling of the laser light at the platform edge. It is caused by the coherent superposition of the illuminating laser field and the SPP polarization field, as described in detail in ref 12, with the periodicity given by the wave vector mismatch between the laser field and the SPP. The quantitative analysis of the pattern

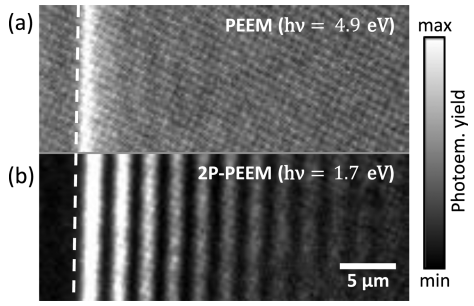

Figure 3. (a) PS/SPO-covered SPP coupling platform imaged in conventional threshold PEEM mode (λ = 253 nm, $h\nu$ = 4.9 eV); (b) identical sample area recorded in the 2P-PEEM mode at excitation with 730 nm laser pulses ($h\nu$ = 1.7 eV). The periodic intensity pattern emerging from the left edge of the SPP coupling platform is indicative for SPP excitation by the laser. The dashed line marks the position of the SPP coupling edge.

periodicity allows determining the real part of the SPP wave vector, k'_{SPP}, so that a scan of the laser wavelength enables the measurement of the SPP dispersion relation $k'_{SPP}(\omega)$.[28,34] The decrease in the pattern amplitude furthermore allows determining the SPP propagation length, i.e., the imaginary part of the SPP wave vector, k''_{SPP}.[28] To demonstrate potential changes in SPP phase and group velocity in response to the switching of the PS/SPO overlayer, we will in the following analyze $k'_{SPP}(\omega)$ as obtained from 2P-PEEM measurements of the sample in the two switching states.

Figure 4a compares 2P-PEEM data in the vicinity of the SPP coupling edge recorded at λ = 740 nm before (top) and after (bottom) illumination of the sample with 365 nm light from a light-emitting diode, i.e., before and after switching of the PS/SPO film (see for reference Figure 1c). The data show a clear change in the pattern periodicity, demonstrating plasmonic switching in k'_{SPP}, i.e., switching of the SPP phase velocity $v_p = \omega/k'_{SPP}$. The quantitative analysis of the pattern yields k'_{SPP} = 10.7 μm^{-1} ($v_p = 0.78c$) for the unswitched state and k'_{SPP} = 10.9 μm^{-1} ($v_p = 0.76c$) for the switched state. Notably, the data analysis does not provide indications for a change in k''_{SPP}, i.e., in the SPP propagation length. Quantitative results for the SPP dispersion relation $k'_{SPP}(\omega)$ in the two switching states obtained from a scan of the wavelength of the excitation laser between 710 and 890 nm are compared in Figure 4b. Over the entire frequency range probed in this experiment we observe changes in k'_{SPP} greater than 0.1 μm^{-1}, with a maximum change of 0.2 μm^{-1} observed for a SPP frequency $\omega \approx 2.5$ fs^{-1}. Upon switching the slope of the dispersion relation also changes, i.e., the SPP group velocity $v_g = d\omega/dk'_{SPP}$. A quantitative analysis yields differences in v_g ranging between −5% and +2% of c for switched and unswitched states at an average value of $v_g \approx 0.5c$ (Figure 4c). The changes in v_p are on the order of 2% of c and show no dependence on ω within the error bars. We would like to add that no indications for a switching induced by the (near-infrared) probing laser due to, for instance, a two-photon absorption process were observed throughout the experiments.

Effective index calculations[35] substantiate the key role of the PS/SPO overlayer for the observed switching of $k'_{SPP}(\omega)$. A common multilayer mode solver was used to calculate the real part of the effective refraction index for SPP coupling, $n'_{eff} = k'_{SPP} \times \lambda/2\pi$, under consideration of the layered sample geometry and the ellipsometry data shown in Figure 1c. Figure 5a compares experimental and calculated results of n'_{eff} for the

DOI: 10.1021/acsphotonics.5b00315
ACS Photonics 2015, 2, 1327−1332

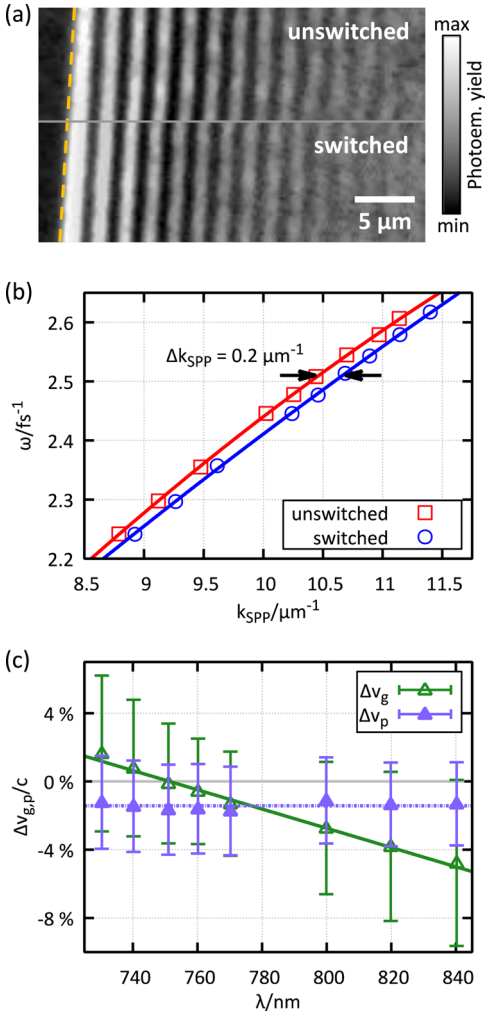

Figure 4. (a) 2P-PEEM images of the SPP intensity pattern next to the left edge of the coupling platform as mapped with 740 nm laser light before (unswitched) and after (switched) illumination of the PS/SPO/gold sample with UV light (λ = 365 nm); the change in the periodicity pattern is indicative of a change in the real part of the SPP wave vector k'_{SPP}. The dashed line indicates the position of the coupling edge. (b) SPP dispersion relation as deduced from 2P-PEEM data recorded for laser excitation between 710 and 890 nm before (unswitched, red) and after (switched, blue) illumination of the PS/SPO/gold sample with UV light (λ = 365 nm); the statistical error of the data lies within the size of the symbols. (c) Observed changes in SPP group and phase velocity, Δv_g and Δv_p, given in percent of c, induced by switching of the dielectric layer over the laser wavelength.

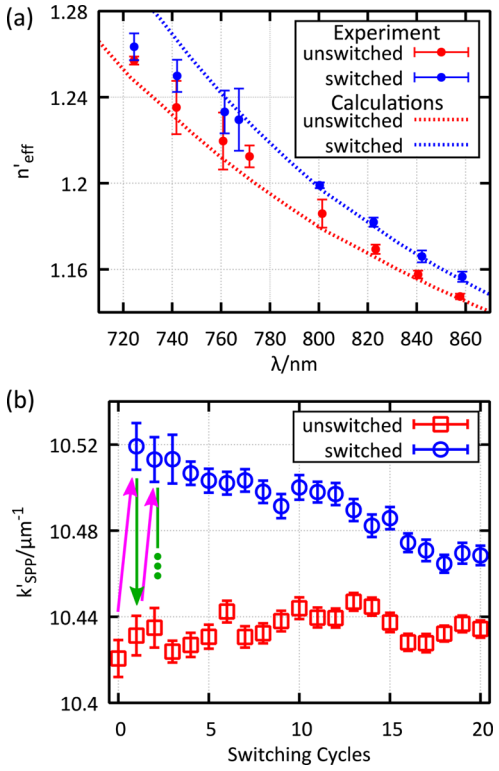

Figure 5. (a) Effective refraction index for SPP coupling, n'_{eff}, as a function of laser excitation wavelength λ as obtained from experiment and effective index simulations in the two switching states; the calculations were performed under consideration of the ellipsometry data shown in Figure 1c. (b) Reversibility check of k'_{SPP} switching for SPP excitation at the PS/SPO/gold interface; switching/back-switching cycles were induced by sequential illumination of the sample with 365 and 532 nm light, respectively, indicated by the colored arrows. Reversibility of the SPP switching process is verified; however, some degree of degradation of the sample is observed.

used PS/SPO film thickness of 60 nm in the two switching states as a function of the excitation laser wavelength λ. The magnitude in the observed changes in n'_{eff} is indeed very well reproduced by the calculations which take the permittivity changes of the PS/SPO film due to the SPO molecular switches into account. The quantitative deviation in n'_{eff} observed at short wavelengths may arise from inhomogeneities in the film thickness of the spin-coated PS/SPO or the slighty different SPO doping level used in the ellipsometry experiments. We observe no significant change of the imaginary part of the effective refraction index, n''_{eff}, in accordance with the absence of changes in k in the relevant wavelength regime.

Figure 5b shows k'_{SPP} data obtained from 2P-PEEM experiments performed at a laser excitation wavelength of 740 nm for a total of 20 switching/back-switching cycles of the PS/SPO overlayer. As observed for the changes in the optical properties (Figure 1b), back-switching of the plasmonic response was possible by illumination with light in the visible spectral regime as well as upon thermal treatment at room temperature over several hours. Here, the back-reaction was induced by illumination with 532 nm light from a continuous wave laser source. The results prove the reversibility of the k'_{SPP}-switching process; however, we also observe a decrease in the switching amplitude, similar to results for plasmonic switching using a PMMA film doped with spiropyran molecules.[26] The decline in the switching capability is most likely due to photodegradation of the SPO molecules by illumination with UV light.[25]

In order to get an understanding of how the switching of k'_{SPP} translates to a situation closer to application, we prepared a model plasmonic lens coated with a PS/SPO film using the same parameters as in the previous measurement. The lens is constructed from an elliptic coupling edge and fabricated by standard electron-beam lithography technique from a continuous, 120 nm thick gold film with a titanium adhesion layer (thickness ~3 nm) supported by a silicon substrate. The specific focusing capabilities of this lens type have been characterized in another 2P-PEEM study before.[36] A scheme of the plasmonic lens design and geometry as well as an optical microscopy image of the lens used in this study (focus length f = 10 μm at n'_{eff} = 1.24 and λ = 740 nm) is shown in Figure 6a.

DOI: 10.1021/acsphotonics.5b00315
ACS Photonics 2015, 2, 1327−1332

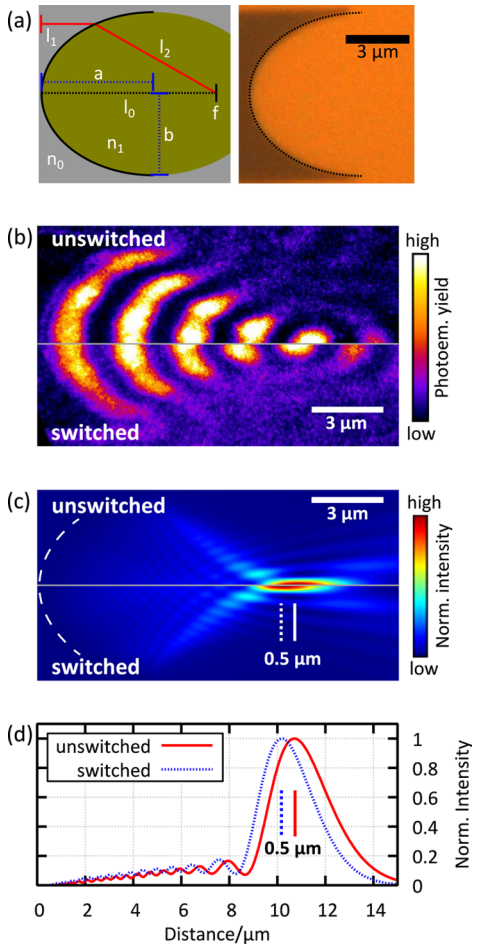

Figure 6. (a) Left: Schematic detailing the construction of the plasmonic lens; n_0 and n_1 are refractive indices of the gray and green medium, respectively, l_0, l_1, and l_2 are optical path lengths, f is the focal length of the lens, a and b are semimajor and semiminor axes, respectively. Right: Optical microscopy image of the fabricated elliptic plasmonic lens; the dotted line marks the coupling edge. (b) 2P-PEEM images of the SPP intensity pattern next to the elliptic coupling edge of a model plasmonic lens as mapped with 740 nm laser light before (unswitched) and after (switched) illumination of the PS/SPO/gold sample with UV light (λ = 365 nm). (c) Reconstructed SPP field intensity plots derived from a fit of the 2P-PEEM images using a Huygens-based simulation approach;[36] a shift of the focal point by ~0.5 μm upon switching is observed. (d) SPP field intensity profiles taken along the optical axis of the reconstructed 2D images shown in (c); the dashed and solid lines in (c) and (d) indicate the position of the intensity maximum of the SPP field for the switched and unswitched state, respectively.

2P-PEEM data for the unswitched (top) and switched (bottom) state of the lens are compared in Figure 6b. The curved profile of the photoemission intensity pattern indicates the focusing of the SPP field. Once again a clear response of the SPP signal to the switching of the PS/SPO overlayer is observed. The most distinct change is the shift of the intensity maximum located at a distance of ~11 μm from the apex of the coupling edge. A Huygens-based simulation approach is used to fit the 2P-PEEM data and reconstruct the SPP field amplitude,[36] thus allowing for quantitative characterization of the SPP focus. Results of the SPP field reconstruction for the two switching states are shown in Figure 6c and d. The analysis yields a focal length of f = 10.7 μm with a depth of field along the optical axis of d = 2.8 μm for the unswitched state. Upon switching, these values change to f = 10.2 μm and d = 2.6 μm, corresponding to relative changes of about 5% for the focal length and 18% for the depth of field. The slight deviation from the 10 μm focal length the lens was constructed for could arise due to slight variations in film thickness and homogeneity that modify n'_{eff} or from imperfections in the geometry of the ellipsis.

CONCLUSIONS

We have shown the possibility to actively and reversibly control the plasmonic phase and group propagation using dielectric films doped with photochromic molecules. The successful realization of a switchable plasmonic lens furthermore illustrates the potential of this concept for the construction of remotely controlled plasmon-optical devices. Yet, the reported switching amplitudes on the order of 0.2 μm^{-1} in k'_{SPP} seem to be small; however, the effects observed for the plasmonic lens are already significant enough to be used to adjust for chromatic aberration. Even more, numerous adjustment parameters for contrast improvement are available, including type of dielectric material and photochromic molecule, filling factor, film thickness, and substrate material. Tailored azobenzene derivates exhibiting substantial changes in the molecular dipole moment upon switching may be a promising alternative to overcome the problem of photodegradation in the switching capabilities. Recent studies also suggested that a photodegradation of spirophenanthrooxazine can be suppressed by the use of a polymer matrix with a high glass temperature.[37]

AUTHOR INFORMATION

Corresponding Author

*E-mail: grossmann@physik.uni-kiel.de.

Notes

The authors declare no competing financial interest.

ACKNOWLEDGMENTS

This work was funded by the German Research Foundation (DFG) through Priority Program 1391 "Ultrafast Nanooptics" and the Collaborative Research Centre 677 "Function by Switching". M.B. also received support from the National Science Foundation Grant No. PHYS-1066293 and the hospitality of the Aspen Center for Physics.

REFERENCES

(1) Kauranen, M.; Zayats, A. V. Nonlinear plasmonics. *Nat. Photonics* **2012**, *6*, 737−748.

(2) Liu, N.; Wen, F.; Zhao, Y.; Wang, Y.; Nordlander, P.; Halas, N. J.; Alù, A. Individual nanoantennas loaded with three-dimensional optical nanocircuits. *Nano Lett.* **2013**, *13*, 142−7.

(3) Halas, N. J. Plasmonics: an emerging field fostered by Nano Letters. *Nano Lett.* **2010**, *10*, 3816−22.

(4) MacDonald, K. F.; Sámson, Z. L.; Stockman, M. I.; Zheludev, N. I. Ultrafast active plasmonics. *Nat. Photonics* **2009**, *3*, 55−58.

(5) Cao, L.; Brongersma, M. L. Active Plasmonics: Ultrafast developments. *Nat. Photonics* **2009**, *3*, 12−13.

(6) Kriesch, A.; Burgos, S. P.; Ploss, D.; Pfeifer, H.; Atwater, H. A.; Peschel, U. Functional Plasmonic Nanocircuits with Low Insertion and Propagation Losses. *Nano Lett.* **2013**, *13*, 4539−45.

(7) Hentschel, M.; Utikal, T.; Giessen, H.; Lippitz, M. Quantitative modeling of the third harmonic emission spectrum of plasmonic nanoantennas. *Nano Lett.* **2012**, *12*, 3778−82.

DOI: 10.1021/acsphotonics.5b00315
ACS Photonics 2015, 2, 1327−1332

(8) Kubo, A.; Onda, K.; Petek, H.; Sun, Z.; Jung, Y. S.; Kim, H. K. Femtosecond Imaging of Surface Plasmon Dynamics in a Nanostructured Silver Film. *Nano Lett.* **2005**, *5*, 1123−7.
(9) Stockman, M. I.; Kling, M. F.; Kleineberg, U.; Krausz, F. Attosecond nanoplasmonic-field microscope. *Nat. Photonics* **2007**, *1*, 539−544.
(10) Aeschlimann, M.; Bauer, M.; Bayer, D.; Brixner, T.; García de Abajo, F. J.; Pfeiffer, W.; Rohmer, M.; Spindler, C.; Steeb, F. Adaptive subwavelength control of nano-optical fields. *Nature* **2007**, *446*, 301−4.
(11) Rewitz, C.; Keitzl, T.; Tuchscherer, P.; Huang, J.-S.; Geisler, P.; Razinskas, G.; Hecht, B.; Brixner, T. Ultrafast Plasmon Propagation in Nanowires Characterized by Far-Field Spectral Interferometry. *Nano Lett.* **2012**, *12*, 45−9.
(12) Kubo, A.; Pontius, N.; Petek, H. Femtosecond microscopy of surface plasmon polariton wave packet evolution at the silver/vacuum interface. *Nano Lett.* **2007**, *7*, 470−5.
(13) Ropers, C.; Neacsu, C. C.; Elsaesser, T.; Albrecht, M.; Raschke, M. B.; Lienau, C. Grating-Coupling of Surface Plasmons onto Metallic Tips: A Nanoconfined Light Source. *Nano Lett.* **2007**, *7*, 2784−8.
(14) Lemke, C.; Leißner, T.; Evlyukhin, A.; Radke, J. W.; Klick, A.; Fiutowski, J.; Kjelstrup-Hansen, J.; Rubahn, H.-G.; Chichkov, B.; Reinhardt, C.; Bauer, M. The Interplay between Localized and Propagating Plasmonic Excitations Tracked in Space and Time. *Nano Lett.* **2014**, *14*, 2431−5.
(15) Vasa, P.; Wang, W.; Pomraenke, R.; Lammers, M.; Maiuri, M.; Manzoni, C.; Cerullo, G.; Lienau, C. Real-time observation of ultrafast Rabi oscillations between excitons and plasmons in metal nanostructures with J-aggregates. *Nat. Photonics* **2013**, *7*, 128−132.
(16) Gruber, C.; Trügler, A.; Hohenau, A.; Hohenester, U.; Krenn, J. R. Spectral Modifications and Polarization Dependent Coupling in Tailored Assemblies of Quantum Dots and Plasmonic Nanowires. *Nano Lett.* **2013**, *13*, 4257−62.
(17) Krasavin, A. V.; Zheludev, N. I. Active plasmonics: Controlling signals in Au/Ga waveguide using nanoscale structural transformations. *Appl. Phys. Lett.* **2004**, *84*, 1416−1418.
(18) Nikolajsen, T.; Leosson, K.; Bozhevolnyi, S. I. Surface plasmon polariton based modulators and switches operating at telecom wavelengths. *Appl. Phys. Lett.* **2004**, *85*, 5833−5835.
(19) Lereu, A. L.; Passian, A.; Goudonnet, J.-P.; Thundat, T.; Ferrell, T. L. Optical modulation processes in thin films based on thermal effects of surface plasmons. *Appl. Phys. Lett.* **2005**, *86*, 154101.
(20) Pacifici, D.; Lezec, H. J.; Atwater, H. A. All-optical modulation by plasmonic excitation of CdSe quantum dots. *Nat. Photonics* **2007**, *1*, 402−406.
(21) Krasavin, A. V.; Vo, T. P.; Dickson, W.; Bolger, P. M.; Zayats, A. V. All-Plasmonic Modulation via Stimulated Emission of Copropagating Surface Plasmon Polaritons on a Substrate with Gain. *Nano Lett.* **2011**, *11*, 2231−2235.
(22) Krasavin, A. V.; Zayats, A. V. Photonic Signal Processing on Electronic Scales: Electro-Optical Field-Effect Nanoplasmonic Modulator. *Phys. Rev. Lett.* **2012**, *109*, 053901.
(23) Such, G.; Evans, R. A.; Yee, L. H.; Davis, T. P. Factors Influencing Photochromism of Spiro-Compounds Within Polymeric Matrices. *J. Macromol. Sci., Polym. Rev.* **2003**, *43*, 547−579.
(24) Lokshin, V.; Samat, A.; Metelitsa, A. V. Spirooxazines: synthesis, structure, spectral and photochromic properties. *Russ. Chem. Rev.* **2002**, *71*, 893−916.
(25) Salemi, C.; Giusti, G.; Guglielmetti, R. DABCO effect on the photodegradation of photochromic compounds in spiro[indoline-pyran] and spiro[indoline-oxazine] series. *J. Photochem. Photobiol., A* **1995**, *86*, 247−252.
(26) Pala, R. A.; Shimizu, K. T.; Melosh, N. A.; Brongersma, M. L. A nonvolatile plasmonic switch employing photochromic molecules. *Nano Lett.* **2008**, *8*, 1506.
(27) Rudé, M.; Simpson, R. E.; Quidant, R.; Pruneri, V.; Renger, J. Active Control of Surface Plasmon Waveguides with a Phase Change Material. *ACS Photonics* **2015**, *2*, 669−674.
(28) Lemke, C.; Leißner, T.; Klick, A.; Fiutowski, J.; Radke, J. W.; Kjelstrup-Hansen, J.; Rubahn, H.-G.; Bauer, M. The complex dispersion relation of surface plasmon polaritons at gold/para-hexaphenylene interfaces. *Appl. Phys. B: Lasers Opt.* **2014**, *116*, 585.
(29) Swiech, W.; Fecher, G.; Ziethen, C.; Schmidt, O.; Schönhense, G.; Grzelakowski, K.; Schneider, C. M.; Frömter, R.; Oepen, H.; Kirschner, J. Recent progress in photoemission microscopy with emphasis on chemical and magnetic sensitivity. *J. Electron Spectrosc. Relat. Phenom.* **1997**, *84*, 171.
(30) Edelstein, A.; Amodaj, N.; Hoover, K.; Vale, R.; Stuurman, N. Computer control of microscopes using μManager. *Curr. Protoc. Mol. Biol.* **2010**, 14.20.1−14.20.17.
(31) Schindelin, J.; Arganda-Carreras, I.; Frise, E.; Kaynig, V.; Longair, M.; Pietzsch, T.; Preibisch, S.; Rueden, C.; Saalfeld, S.; Schmid, B.; Tinevez, J.-Y.; White, D. J.; Hartenstein, V.; Eliceiri, K.; Tomancak, P.; Cardona, A. Fiji: an open-source platform for biological-image analysis. *Nat. Methods* **2012**, *9*, 676−682.
(32) Jamali, M.; Keshavarz Hedayati, M.; Mozooni, B.; Javaherirahim, M.; Abdelaziz, R.; Usman Zillohu, A.; Elbahri, M. Photoresponsive Transparent Conductive Metal with a Photobleaching Nose. *Adv. Mater.* **2011**, *23*, 4243−4247.
(33) Hedayati, M. K.; Javaheri, M.; Zillohu, A. U.; El-Khozondar, H. J.; Bawa'aneh, M. S.; Faupel, F.; Elbahri, M.; Lavrinenko, A. Photo-driven Super Absorber as an Active Metamaterial with a Tunable Molecular-Plasmonic Coupling. *Adv. Opt. Mater.* **2014**, *2*, 705−710.
(34) Shibuta, M.; Eguchi, T.; Nakajima, A. Imaging and Characterizing Long-Range Surface Plasmon Polaritons Propagating in a Submillimeter Scale by Two-Color Two-Photon Photoelectron Emission Microscopy. *Plasmonics* **2013**, *8*, 1411−1415.
(35) Holmgaard, T.; Bozhevolnyi, S. Theoretical analysis of dielectric-loaded surface plasmon-polariton waveguides. *Phys. Rev. B: Condens. Matter Mater. Phys.* **2007**, *75*, 245405.
(36) Lemke, C.; Schneider, C.; Leißner, T.; Bayer, D.; Radke, J. W.; Fischer, A.; Melchior, P.; Evlyukhin, A. B.; Chichkov, B. N.; Reinhardt, C.; Bauer, M.; Aeschlimann, M. Spatiotemporal Characterization of SPP Pulse Propagation in Two-Dimensional Plasmonic Focusing Devices. *Nano Lett.* **2013**, *13*, 1053.
(37) Elbahri, M.; Zillohu, A. U.; Gothe, B.; Hedayati, M. K.; Abdelaziz, R.; El-khozondar, J.; Bawa'aneh, M.; Abdelaziz, M.; Lavrinenko, A.; Zhukovsky, S. Photoswitchable Molecular Dipole Antennas with Tailored Coherent Coupling in Glassy Composite. *Light: Sci. Appl.* **2015**, *4* (8), e316.

DOI: 10.1021/acsphotonics.5b00315
ACS Photonics 2015, 2, 1327−1332